



HAL
open science

Reactive Astrocytes Overexpress TSPO and Are Detected by TSPO Positron Emission Tomography Imaging

Sonia Lavissee, Martine Guillermier, Anne-Sophie Herard, Fanny Petit, Marion Delahaye, Nadja Van Camp, Lucile Ben Haim, Vincent Lebon, Philippe Remy, Frédéric Dollé, et al.

► To cite this version:

Sonia Lavissee, Martine Guillermier, Anne-Sophie Herard, Fanny Petit, Marion Delahaye, et al.. Reactive Astrocytes Overexpress TSPO and Are Detected by TSPO Positron Emission Tomography Imaging. *Journal of Neuroscience*, 2012, 32 (32), pp.10809-10818. 10.1523/JNEUROSCI.1487-12.2012 . hal-02110993

HAL Id: hal-02110993

<https://hal.science/hal-02110993>

Submitted on 17 May 2019

HAL is a multi-disciplinary open access archive for the deposit and dissemination of scientific research documents, whether they are published or not. The documents may come from teaching and research institutions in France or abroad, or from public or private research centers.

L'archive ouverte pluridisciplinaire **HAL**, est destinée au dépôt et à la diffusion de documents scientifiques de niveau recherche, publiés ou non, émanant des établissements d'enseignement et de recherche français ou étrangers, des laboratoires publics ou privés.

The Journal of Neuroscience

<http://jneurosci.msubmit.net>

Reactive astrocytes overexpress TSPO and are detected by TSPO PET imaging

JN-RM-1487-12R1

Carole Escartin, CEA CNRS URA2210

Sonia Lavisse, CEA CNRS URA2210

Martine Guillermier,

Anne-Sophie Hérard, CEA

Fanny Petit, CEA

Marion Delahaye, CEA CNRS URA2210

Nadja Van camp, CEA CNRS URA2210

Lucile Ben Haim, CEA CNRS URA2210

Vincent Lebon, CEA-CNRS

Philippe Remy, CEA CNRS URA2210

Frédéric Dollé, CEA, Service Hospitalier Frederic Joliot

Thierry Delzescaux, Service Hospitalier Frederic Joliot

Gilles Bonvento, MIRCen

Philippe Hantraye, MIRCen

Commercial Interest: No

Reactive astrocytes overexpress TSPO and are detected by TSPO PET imaging

Sonia Lavis¹, Martine Guillermier^{1,#}, Anne-Sophie Hérard^{1,#}, Fanny Petit^{1,#}, Marion Delahaye¹, Nadja Van Camp¹, Lucile Ben Haim¹, Vincent Lebon¹, Philippe Remy^{1,2}, Frédéric Dollé³, Thierry Delzescaux¹, Gilles Bonvento¹, Philippe Hantraye¹, Carole Escartin¹

¹CEA, DSV, I2BM, MIRcen and CNRS URA2210, Fontenay-aux-Roses, France

²Neurologie, CHU Henri Mondor, AP-HP and UPE-C, Créteil, France

³CEA, DSV, I2BM, Service Hospitalier Frédéric Joliot, Orsay, France

These authors contributed equally to this study

Number of pages: 29

Number of figures: 7

Number of tables: 1

Number of words in Abstract: 246

Number of words in Introduction: 485

Number of words in Discussion: 1374

Author for correspondence

Carole Escartin

CEA CNRS URA 2210

MIRcen

18, route du Panorama

92265 Fontenay-aux-roses

France

Tel: + 33 (0) 1 46 54 83 30

Fax: + 33 (0) 1 46 54 91 16

Email: carole.escartin@cea.fr

Abbreviated title: TSPO radioligands detect reactive astrocytes

Acknowledgments

We are grateful to: Marion Chaigneau, Diane Houitte and Charlène Joséphine for expert technical assistance with animal handling, Yoan Fontyn and Nicolas Souedet for reconstruction of PET data, Dr. Elsa Diguët for help with animal transfer for [¹¹C]SSR180575 imaging sessions; Dr. Nicole Déglon, Noëlle Dufour and Gwennaëlle Auregan for lentiviral vector production and Stéphane Demphel, Stéphane Le Helleix and Tony Catarina for radioligand synthesis. We also thank Dr. Emmanuel Brouillet for stimulating discussions on the project, Dr. Caroline Jan for her assistance to preliminary experiments and Drs. Frank Marguet, Frédéric Puech and Thomas Rooney (Sanofi, Chilly-Mazarin, France) for scientific discussions on the TSPO 18 kDa target and data sharing. Finally, we are extremely grateful to Dr. Makoto Higuchi (National Institute of Radiological Sciences, Chiba, Japan) for sharing his TSPO antibody and for his careful reading of the manuscript.

This work was supported by the European STREP program [Stems, grant number LSHB-CT-2006-037328 to PH]; Agence Nationale de la recherche [grant number ANR-2010-JCJC 1402-1 to CE]; Commissariat à l'Énergie Atomique et aux Énergies Alternatives; and Centre National de la Recherche Scientifique.

Abstract

Astrocytes and microglia become reactive under most brain pathological conditions, making this neuroinflammation process a surrogate marker of neuronal dysfunction. Neuroinflammation is associated with increased levels of translocator protein 18kDa (TSPO) and binding sites for TSPO ligands. Positron emission tomography (PET) imaging of TSPO is thus commonly used to monitor neuroinflammation in preclinical and clinical studies. It is widely considered that TSPO PET signal reveals reactive microglia although a few studies suggested a potential contribution of reactive astrocytes. As astrocytes and microglia play very different roles, it is crucial to determine whether reactive astrocytes can also overexpress TSPO and yield to a detectable TSPO PET signal *in vivo*.

We used a model of selective astrocyte activation through lentiviral gene transfer of the cytokine ciliary neurotrophic factor (CNTF) into the rat striatum, in the absence of neurodegeneration. CNTF induced an extensive activation of astrocytes, which overexpressed GFAP and become hypertrophic, while microglia displayed minimal increase in reactive markers. Two TSPO radioligands [¹⁸F]DPA-714 and [¹¹C]SSR180575 showed a significant binding in the lenti-CNTF-injected striatum that was saturated and displaced by PK11195. The volume of radioligand binding matched the GFAP immuno-positive volume. TSPO mRNA levels were significantly increased and TSPO protein was overexpressed by CNTF-activated astrocytes.

We show that reactive astrocytes overexpress TSPO, yielding to a significant and selective binding of TSPO radioligands. Therefore, caution must be used when interpreting TSPO PET imaging in animals or patients because reactive astrocytes can contribute to the signal in addition to reactive microglia.

Introduction

In response to multiple abnormal situations in the brain, astrocytes and microglia become reactive. This neuroinflammation process involves stereotypic morphological changes and multiple functional alterations (Hanisch and Kettenmann, 2007; Escartin and Bonvento, 2008). Because glial cells activation not only mirrors neuronal dysfunction but can also directly influence disease progression, considerable efforts have been made to develop non-invasive techniques to monitor these cells *in vivo*. Such techniques would enable evaluation of disease progression and therapeutic efficacy in animal models and patients suffering from multiple neurodegenerative diseases.

Positron emission tomography (PET) imaging of the translocator protein 18kDa (TSPO) has been proposed as a potent strategy to monitor neuroinflammation in animals and humans (Chen and Guilarte, 2008). TSPO is expressed by glial cells and is up-regulated under neuroinflammatory conditions (Rupprecht *et al.*, 2010), serving as a biomarker for PET imaging of neuroinflammation using TSPO radioligands. [¹¹C]-(R)-PK11195, was one of the first TSPO-selective radioligand to be developed and has been extensively used in animals and patients for two decades (Venneti *et al.*, 2006; Chauveau *et al.*, 2008). Multiple other TSPO radioligands have since been generated including [¹⁸F]DPA-714 (James *et al.*, 2008) and [¹¹C]SSR180575 (Thominiaux *et al.*, 2010).

Despite the multiplicity of TSPO radioligands available, it is still unclear whether TSPO PET signal arises from reactive astrocytes or microglia. It is generally admitted that microglia are responsible for the signal observed with TSPO radioligands (Venneti *et al.*, 2006; Chauveau *et al.*, 2008; 2009). However, an original study reported that astrocytes overexpress TSPO (Kuhlmann and Guilarte, 2000) and a few others have suggested their potential contribution to the TSPO PET signal (Rojas *et al.*, 2007; Ji *et al.*, 2008). The major limitation of PET studies exploring TSPO expression is the animal model (intracerebral injection of neurotoxins, ischemia, transgenic mice) or the clinical disease considered. Most of them display activation of both astrocytes and microglia, limiting the interpretation of PET data. Additional confounding factors include neuronal degeneration, blood brain barrier disruption and peripheral

immune cell recruitment. Determining the relative contribution of each cell type to the PET signal is therefore difficult and it remains to be established whether reactive astrocytes give rise to a detectable TSPO PET signal, in absence of reactive microglia and neurodegeneration. It is also crucial to assess whether TSPO PET imaging allows discrimination of reactive microglia from reactive astrocytes, as these two cell types play very distinct functions and may influence disease progression in opposite ways.

For this purpose, we have developed a model of selective activation of astrocytes through lentiviral gene transfer of the cytokine ciliary neurotrophic factor (CNTF) in the rat brain, in the absence of detectable microglia reactivity, neuronal degeneration or any additional pathological process (Escartin *et al.*, 2006; 2007; Beurrier *et al.*, 2010). We used this unique model to assess whether reactive astrocytes can overexpress TSPO and generate a detectable TSPO PET signal using two recently-developed and on-site available TSPO radioligands, [¹⁸F]DPA-714 and [¹¹C]SSR180575.

Material and Methods

Reagents and animals

All reagents came from Sigma (Lyon, France) unless otherwise specified. All animal experimental procedures were performed in strict accordance with the French regulation (Code Rural R214/87 to R214/130), the recommendations of the EEC (86/609/EEC) for care and use of laboratory animals and conformed to the ethical guidelines of the French National Charter on the ethic of animal experimentation. The animal facility is accredited by the French authorities (Veterinary Inspectors) under the number B9-032-02.

Lentivirus injection

We used self-inactivated lentiviruses that encode either the human CNTF gene (“lenti-CNTF”) with the export sequence of immunoglobulin or the β -galactosidase gene (“lenti-LacZ”) under the control of the mouse phosphoglycerate kinase 1 promoter, as described previously (Escartin *et al.*, 2006).

Male Sprague-Dawley rats (2-month-old) were anesthetized with a mixture of ketamine (75 mg/kg) and xylazine (10 mg/kg). Suspensions of lentiviral vector (2 μ l, 100 ng p24/ μ l, diluted in PBS with 1% BSA) were injected into the striatum at a rate of 0.2 μ l/min, using a 34-gauge blunt-tip needle linked to a Hamilton syringe by a polyethylene catheter. Rats were injected with lenti-LacZ and lenti-CNTF in the left and right striatum respectively. The stereotaxic coordinates were, from bregma: anteroposterior +0.5 mm; lateral \pm 3 mm; and ventral -4.5 mm from the dura, with tooth bar set at -3.3 mm. At the end of the injection, the needle was left in place for 5 min before being slowly removed. The skin was sutured and rats were allowed to recover for at least 2 months before being scanned. Rats were analyzed between 2 and 6 months after injection, as CNTF effects were shown to be stable for at least 6 months (Escartin *et al.*, 2006).

To serve as a positive control for neuroinflammation involving both reactive astrocytes and microglia (Ryu *et al.*, 2005), we injected 9 rats with 80 nmol of quinolinate (QA) in the striatum, as described previously (Beurrier *et al.*, 2010). After 2 weeks, 8 rats were perfused and one rat had its brain frozen, as described below (see Immunohistology).

Radioligand synthesis

[¹⁸F]DPA-714. Ready-to-inject, >99% radiochemically pure [¹⁸F]DPA-714 (*N,N*-diethyl-2-(2-(4-(2-[¹⁸F]fluoroethoxy)phenyl)-5,7-dimethylpyrazolo[1,5-*a*]pyrimidin-3-yl)acetamide) was prepared from cyclotron-produced [¹⁸F]fluoride (Cyclone-18/9 cyclotron, IBA, Louvain-la-Neuve, Belgium) on the basis of already published standard conditions (Damont *et al.*, 2008; James *et al.*, 2008) using a TRACERLab™ FX-FN synthesizer (GEMS, Buc, France). Radiolabeling of DPA-714 with fluorine-18 uses a tosyloxy-for-fluorine nucleophilic aliphatic substitution (one-step process) and its preparation includes the following five stages : (1) dilution of the no-carrier-added, dried (activated) K[¹⁸F]F-Kryptofix®222 complex (prepared from [¹⁸F]fluoride, potassium carbonate and Kryptofix®222) with 700 µl of dimethylsulfoxide containing 3.5 to 4.5 mg of the tosyloxy precursor for labeling (*N,N*-diethyl-2-(2-(4-(2-toluenesulfonyloxyethoxy)phenyl)-5,7-dimethylpyrazolo[1,5-*a*]pyrimidin-3-yl)acetamide) ; (2) heating the reaction mixture at 160°C for 5 min ; (3) dilution of the reaction mixture with the HPLC mobile phase and pre-purification on a SepPak® Alumina N™ cartridge ; (4) HPLC purification on a semi-preparative Waters X-Terra™ C-18 column (eluent 0.1M aq. ammonium acetate (pH 10) / acetonitrile : 60 / 40 (v:v)) and (5) SepPak® Plus C-18 cartridge-based removal of the HPLC solvents. [¹⁸F]DPA-714, as an ethanolic (15%) physiological saline solution (6.7 to 8.5 GBq batches, 10 ml-volume), is routinely obtained within 50-55 min starting from 35 GBq of [¹⁸F]fluoride (19-24% non-decay-corrected overall isolated yields) with specific radioactivities ranging from 74 to 222 GBq/µmol.

[¹¹C]SSR180575. Ready-to-inject, >99% radiochemically pure [¹¹C]SSR180575 (7-chloro-*N,N*-dimethyl-5-[¹¹C]methyl-4-oxo-3-phenyl-3,5-dihydro-4*H*-pyridazino[4,5-*b*]indole-1-acetamide) was prepared from

cyclotron-produced [^{11}C]carbon dioxide (Cyclone-18/9 cyclotron, IBA) using a TRACERLabTM FX-C synthesizer (GEMS) as described before (Thominiaux *et al.*, 2010). SSR180575 was labeled with carbon-11 at its 5-methylpyridazino[4,5-*b*]indole moiety by methylation of the corresponding *nor*-analogue with [^{11}C]methyl triflate. Its preparation includes the following six stages : (1) trapping at -40°C of [^{11}C]methyl triflate (radiosynthesized from cyclotron-produced [^{11}C]carbon dioxide *via* [^{11}C]methyl iodide) in 400 μl of DMF containing 0.6 to 0.9 mg of the precursor for labeling (7-chloro-*N,N*-dimethyl-4-oxo-3-phenyl-3,5-dihydro-4*H*-pyridazino[4,5-*b*]indole-1-acetamide) and finely powdered K_2CO_3 (1.5 to 2.5 mg) ; (2) heating the reaction mixture at 120°C for 2 min ; (3) concentration to dryness under reduced pressure and helium flow ; (4) dilution of the residue with 1 ml of the HPLC mobile phase ; (5) HPLC purification on a semi-preparative Waters Symmetry[®] C-18 column (eluent : water / acetonitrile / trifluoroacetic acid : 50 / 50 / 0.1 (v:v:v)) and (6) SepPak[®] Plus cartridge-based removal of the HPLC solvents. [^{11}C]SSR180575, as an ethanolic (15%) physiological saline solution (4.8 to 6.7 GBq batches, 10 ml-volume), is routinely obtained within 40 min starting from 74 GBq of [^{11}C]carbon dioxide (6.5-9.1% non-decay-corrected overall isolated yields) with specific radioactivities ranging from 37 to 185 GBq/ μmol . Quality controls were performed on an aliquot of the ready-to-inject [^{18}F]DPA-714 or [^{11}C]SSR180575 preparation, in compliance with our in-house quality control/assurance specifications.

Positron Emission Tomography (PET)

Rats ($m = 502 \pm 59$ g) were scanned on a Concorde Focus 220 camera (Siemens, Knoxville, TN) dedicated to small animal imaging with a spatial resolution of 1.35-mm Full Width at High Maximum. They were imaged within 2 to 6 months post CNTF-injection, using [^{18}F]DPA-714 ($n=6$) or [^{11}C]SSR180575 ($n=4$) as radioligand. Displacement and pre-saturation studies with unlabeled PK11195 were also performed on one rat in each group. Solutions of (*R,S*)-PK11195 were freshly prepared by dissolving it in DMSO, followed by dilution, first with PEG400 and then with physiological saline, and were intravenously injected within 2 h. For displacement experiments, unlabeled PK11195 (1 mg/kg) was intravenously

injected 15 and 20 min after injection of [¹⁸F]DPA-714 and [¹¹C]SSR180575, respectively. For pre-saturation experiments, unlabeled PK11195 (2 and 5 mg/kg for [¹⁸F]DPA-714 and [¹¹C]SSR180575 respectively) was intravenously injected 5 min before injection of radioligands.

Anesthesia was induced with 5% isoflurane and maintained by 2 to 2.5% of isoflurane in 100% O₂. Animals were placed within the scanner using a home-made stereotactic frame compatible with PET acquisition in prone position and were kept at 37°C using a heating blanket (Harvard Apparatus Limited, Edenbridge, UK). Concomitantly with a bolus injection of [¹⁸F]DPA-714 or [¹¹C]SSR180575 (1.83 ± 0.33 mCi and 2.00 ± 0.27 mCi respectively) via a 26-gauge catheter in the tail vein, a 90-min emission scan was performed with an energy window of 400–650 keV and a coincidence time window of 6 ns. The data files for the list-mode acquisition were displayed as 3D sinograms with a maximum ring difference of 47 and a span of 3. Finally, each emission sinogram was normalized, corrected (for attenuation and radioactivity decay) and reconstructed with a FORE plus OSEM-2D algorithm (16 subsets, 4 iterations).

Magnetic resonance imaging (MRI)

MRI was used to confirm the injection site, to exclude animals with detectable edema at the injection site (1 out of 10 animals in this study) and to define anatomical regions of interest (ROI) through PET/MRI co-registration. MRI was performed on a 7-Tesla horizontal system (Varian-Agilent Technologies, Santa Clara, CA) equipped with a gradient coil reaching 600 mT/m (120 μs rise time), a radiofrequency birdcage 1H coil for transmission, and a 4-channel surface receive coil (Rapid Biomedical, Rimpfing, Germany).

Animals were anesthetized using 2% isoflurane in 100% O₂ and fixed by mouth and ear bars to a stereotactic MRI-compatible rodent frame. Once in the magnet, animals were heated by a hot air flux and their temperature and respiration parameters monitored. T2-weighted images were acquired using a fast spin-echo sequence with the following parameters: TE/TR = 20/7000 ms, field of view = 38.4 x 38.4

mm and matrix = 256 x 256 resulting in a 150 x 150 μm in plane resolution, 106 coronal slices with 300 μm thickness, sampling spectral width of 90 kHz and acquisition time of 37 min.

PET data analysis

PET time frames collected were summed and manually co-registered to the T2-weighted MRI for each animal, using rigid transformations. Co-aligned MR images were used to define ROI (left striatum = lenti-LacZ and right striatum = lenti-CNTF), based on anatomical landmarks, using an in-house image processing software (Anatomist, visualization tool of BrainVISA, <http://www.brainvisa.info>). This process was performed by the same operator for all experiments. ROIs were of $45.54 \pm 3.86 \text{ mm}^3$ and $45.48 \pm 5.07 \text{ mm}^3$, respectively for lenti-LacZ and lenti-CNTF injected striata. The mean activity concentration values in the left and right ROIs were calculated and used to obtain regional time activity curves (TAC). These curves were then normalized for injected dose and body weight and expressed as percent standardized uptake values : $\%SUV = [100 \times \text{ROI values (Bq/ml)}] / [(\text{injected dose (mCi)} \times 37.10^6) / \text{body weight (g)}]$.

Immunohistology

Two to twelve days after PET scan, rats were euthanized with an overdose of pentobarbital and their brains were rapidly collected and frozen in isopentane at -30°C . Frozen brains were embedded in a home-made green medium and entirely cut into 20- μm -thick coronal sections using a cryostat. Every fifth section, a blockface photograph (*i.e.* picture of the brain surface) was recorded using a digital camera (high in-plane resolution of $30 \times 30 \mu\text{m}^2$), to serve as a reference for *postmortem* image 3D reconstruction. Ten series of tissue sections encompassing the entire striatum were collected and mounted on Superfrost glass slides.

After post-fixation of frozen sections in 4% paraformaldehyde for 4 h, DAB immunohistochemistry was performed with an automated immunostaining system (Ventana-Roche Discovery XT Medical S.A,

Illkirch, France), according to the manufacturer's instructions. The following primary antibodies were used: GFAP (Dako, 1:1000, Carpinteria, CA), ED1/CD68 (Serotec, 1:100, Raleigh, NC), IBA1 (Wako, 1:250, Richmond, VA) and, Vimentin (Calbiochem, 1:100, San Diego, CA). Stained sections were digitized and staining intensity (measured as optical density after background subtraction) was evaluated in the striatum on 6-8 slices per rat, using a computer based image analysis system (MCID Analysis, St Catharines, ON, Canada). The number of IBA1-positive cells was counted under the 40x objective of a microscope on 8 fields of view taken from 2 sections per rat.

Two additional rats injected with lenti-LacZ and lenti-CNTF respectively in the left and right striatum, were transcardially perfused with 4% paraformaldehyde under pentobarbital anesthesia. After immersion for 24 h in a 20% sucrose solution, brains were cut into 40- μ m coronal sections using a freezing microtome. Double or triple fluorescent immunostainings were performed on floating sections as described previously (Escartin *et al.*, 2006). We used primary antibodies directed against GFAP (Sigma, 1:1000), IBA1 (1:500), OX42/CD11b (MRC275, 1:1000, Serotec), TSPO (NP155, a kind gift from Dr. Higuchi) and Vimentin (1:1000, ab24525, Abcam, Paris, France). Images of stained sections were taken with a confocal microscope (LSM 510; Zeiss, Thornwood, NY). The TSPO antibody was previously validated by western blot and immunofluorescence (Ji *et al.*, 2008). Furthermore, negative controls were performed by omission of primary antibodies and produced no significant staining.

Postmortem image registration and 3D reconstruction

Two series of GFAP-labeled histological sections were digitized as 24-bits colour images using a high resolution flatbed scanner (ImageScanner III; GE Healthcare Europe, Orsay, France) with a 1200 dpi in-plane resolution (pixel size $21 \times 21 \mu\text{m}^2$) in order to be reconstructed in 3D. Image processing was performed using our in-house image processing and visualization software package BrainVISA/Anatomist. GFAP histological volume was reconstructed in 3D using the photographic volume as geometrical reference, after correction of individual slice-specific 2D deformations. First, blockface

photographs were automatically segmented to separate brain tissue from embedding medium, as previously described (Dubois *et al.*, 2007). Series of segmented photographs were then stacked in the Z-direction to create a photographic volume of the whole brain spatially coherent (resolution of $0.03 \times 0.03 \times 0.1 \text{ mm}^3$). Then, digitized GFAP-labeled sections were stacked in the Z-direction using BrainRAT module of BrainVISA. Each section of the stacked histological volume, encompassing the striatum, was then co-registered with its corresponding blockface photograph using the Blockmatching registration method (Ourselin *et al.*, 2001). This registration process based on a 2D affine transformation was repeated for all available sections to obtain a spatially consistent GFAP histological volume (resolution of $0.021 \times 0.021 \times 0.1 \text{ mm}^3$).

Reverse transcriptase - quantitative polymerase chain reaction (RT-qPCR)

Five rats injected with lenti-LacZ and lenti-CNTF in the left and right striatum respectively were sacrificed under pentobarbital anesthesia. Rat brains were rapidly collected and each striatum was dissected out on ice from 1 mm coronal slices and stored in RNAlater (Sigma) until further processing. Total RNA was isolated from striatal samples with Trizol (Invitrogen, Carlsbad, CA), purified on RNA clean-up columns and residual DNA was digested by on-column treatment with DNase (Macherey-Nagel, Bethlehem, PA). cDNA was synthesized from 0.5 μg RNA using the RT² PCR Array First Strand kit from SABiosciences (Frederick, MD) following manufacturer's instructions. cDNA was mixed with the RT² Real Time SYBR Green PCR mix (SABiosciences) and dispensed in a custom-made qPCR array plate containing specific primers for a gene of interest in each well (see gene list in Table 1). For each sample (i.e. plate), we checked that the three quality controls (absence of contamination with genomic DNA, efficiency of RT and qPCR reactions) were fulfilled, according to the manufacturer's instructions. Three genes (*IL-1 β* , *IFN γ* and *Ccl2*) could not be detected in any or several samples and thus were not analyzed. The abundance of the gene of interest was normalized to the abundance of the housekeeping gene *Actin* using the ΔCt method. *Actin*, as well as additional housekeeping genes (*GAPDH*, *LDH*) studied on the PCR

array plate, were not different between the two groups. An additional qPCR was performed on these striatal cDNA samples using specific primers against rat *TSPO* (forward primer: GCTGCCCGCTTGCTGTATCCT, reverse primer: CCCTCGCCGACCAGAGTTATCA). *TSPO* abundance was normalized to the abundance of cyclophilin A in each sample (forward primer: ATGGCAAATGCTGGACCAAA, reverse primer: GCCTTCTTTCACCTTCCCAA).

Western blots

Three rats injected with lenti-LacZ and lenti-CNTF in the left and right striatum respectively were sacrificed under pentobarbital anesthesia. Striata were rapidly dissected out on ice and homogenized in 50 mM Tris-HCl, pH 7.4, 100 mM NaCl, 1% SDS, with protease inhibitor cocktail (Roche, Indianapolis, IN). Western blots were performed using ECL detection as previously described (Escartin *et al.*, 2011) using antibodies against actin (1 : 5000) and *TSPO* (1 : 500).

Statistical analysis

Data are expressed as mean \pm S.E.M. N indicates the number of rats. Left-right comparisons were performed using paired *t*-test. TACs for [¹⁸F]DPA-714 and [¹¹C]SSR180575 were analyzed by two-way repeated-measures ANOVA (time, injected side).

Results

CNTF selectively activates astrocytes

We have previously reported that lentivirus-mediated gene transfer of the cytokine CNTF in the rat striatum activates astrocytes but has no detectable effects on microglia and neurons (Escartin *et al.*, 2006). To further characterize our model of selective activation of astrocytes in the rodent brain, we used RT-qPCR array to quantify the expression of several markers of neuroinflammation (Table 1). The effects of lenti-CNTF were compared to lenti-LacZ, which does not induce neuroinflammation or non specific effects in the brain compared to vehicle injection, as previously demonstrated by multiple histological and functional indexes (Escartin *et al.*, 2006; 2007).

Here, we found that CNTF induced a strong expression of two classic markers of astrocyte reactivity: vimentin and GFAP (8.3 and 12.7 fold respectively vs lenti-LacZ, $p < 0.005$, paired *t*-test, Table 1 and Figure 1A). In contrast to its strong effect on astrocytes, CNTF did not significantly change the mRNA levels of reactive microglia markers IBA1 and CD11b (respectively 1.4 and 1.7 fold vs lenti-LacZ, $p > 0.05$, paired *t*-test). CNTF also produced a small increase in the mRNA levels of the pro-inflammatory cytokine TNF α (2 fold vs lenti-LacZ rats, $p < 0.05$, paired *t*-test) and a significant yet minimal increase in Noxa1 mRNA levels (1.2 fold vs lenti-LacZ, $p < 0.005$, paired *t*-test). Finally, CNTF significantly decreased the expression of Ncf2 and Ptgs2 (respectively $p < 0.05$ and $p < 0.005$, paired *t*-test). Many other neuroinflammation markers such as cytokines, chemokines and reactive oxygen species-producing enzymes, remained unchanged (Table 1), confirming the selective activation of astrocytes by lenti-CNTF. Additionally, immunostaining demonstrated that CNTF induced a strong activation of astrocytes and minimal microglial activation. We observed a significant increase in GFAP and vimentin immunoreactivity in the striatum injected with lenti-CNTF (respectively 2.2 and 3.2 fold vs lenti-LacZ, $p < 0.005$, Figure 1B, C, F). Consistent with a restricted activation of microglia with lenti-CNTF, there was only a non significant increase in IBA1 staining in the lenti-CNTF injected striatum (Figure 1D, F) and a

small increase in ED1/CD68, a marker of reactive microglia (1.2 fold, $p < 0.05$, Figure 1E, F). As a positive control, we confirmed that these microglia markers were strongly induced by QA (data not shown), an excitotoxin known to induce significant neuroinflammatory responses (Ryu *et al.*, 2005). We observed an increase in the number of IBA1-positive cells in the lenti-CNTF injected striatum (1.8 fold, $p < 0.05$ vs lenti-LacZ) but that remained marginal compared to the one induced by QA (5.9 fold, $p < 10^{-5}$, data not shown).

To further analyze morphological changes induced by CNTF in astrocytes and microglia, we used confocal fluorescent microscopy on thicker sections. In the lenti-CNTF injected striatum, astrocytes displayed typical features of reactivity: they were hypertrophic and expressed high levels of GFAP (Figure 1G). On the contrary, IBA1-positive microglia displayed a normal resting morphology with thin processes, very different from amoeboid microglia observed in the QA-injected striatum (Figure 1G).

The characterization of CNTF effects at the mRNA, protein and cellular level demonstrated its selective activation of astrocytes with minimal effects on microglia.

[¹⁸F]DPA-714 and [¹¹C]SSR180575 display specific binding to the lenti-CNTF injected striatum

Both [¹⁸F]DPA-714 and [¹¹C]SSR180575 displayed an increased uptake in the striatum injected with lenti-CNTF, as compared to the contralateral side injected with lenti-LacZ (Figure 2A, B). As shown by the TACs of [¹⁸F]DPA-714, the peak was reached within 2 min following injection on both sides (Figure 2C). The maximum uptake of [¹¹C]SSR180575 appeared as a short plateau, 2-5 min after injection (Figure 2D). In the lenti-CNTF injected striatum, maximal uptake of [¹⁸F]DPA-714 was followed by a rapid wash out (-30% of maximal uptake at 20 min post-injection). This wash-out was slower for [¹¹C]SSR180575 (-9% of maximal uptake at 20 min post-injection). For both radioligands, wash-in and wash-out phases were more rapid in the lenti-LacZ than in the lenti-CNTF injected striatum, and pharmacokinetics differed significantly depending on the injected lentivirus (time x injected side, $p < 10^{-4}$, two-way repeated-measures ANOVA). Both radioligands highlighted a strong significant difference between the lenti-CNTF

and lenti-LacZ side ($p < 10^{-4}$, two-way repeated-measures ANOVA). Within 30 and 90 min after radioligand administration, the averaged uptake ratio in the lenti-CNTF versus the lenti-LacZ injected striatum was higher for [^{11}C]SSR180575 (3.35 ± 0.87) as compared to [^{18}F]DPA-714 (2.29 ± 0.67), although not significantly ($p = 0.09$, unpaired t -test).

The binding selectivity for TSPO was tested for each radioligand by pre-saturation and displacement studies using an excess of the reference ligand PK11195. These experiments were performed on the same rat, using the baseline acquisition as the reference. Following pre-saturation with unlabeled PK11195, the uptake of both radioligands into the striatum was faster and higher than observed in the baseline experiment. A faster wash-out reduced radioligand uptake to background levels for both sides (Figure 3A, B). This higher initial uptake of radioactivity at pre-saturation with PK11195 is common with TSPO radioligands, as it also blocks peripheral TSPO binding sites, inducing a higher plasma level of the free radioligands (Venneti *et al.*, 2006). Displacement studies were performed by injection of unlabeled PK11195 (1 mg/kg), 15 and 20 min following injection of [^{18}F]DPA-714 and [^{11}C]SSR180575. Injection of PK11195 induced a fast decline of both [^{18}F]DPA-714 and [^{11}C]SSR180575 binding in the lenti-CNTF-injected striatum (Fig. 3A, 3B, 4). Displacement reduced the signal to background level comparable to pre-saturation, but was faster for [^{18}F]DPA-714 (5 min) than [^{11}C]SSR180575 (10 min) (Figure 3B). Displacement was observed in both striata though to a much lesser extent in the lenti-LacZ side (Figure 3A, B).

TSPO is overexpressed by CNTF-activated astrocytes

To demonstrate that the PET signal in the lenti-CNTF injected striatum anatomically matches the area immunopositive for GFAP, we reconstructed serial brain sections labeled for GFAP in 3D using a block photograph reference volume (see Methods). Volume of [^{18}F]DPA-714 binding coincided with the GFAP-positive volume (Figure 5) and a similar pattern was observed for [^{11}C]SSR180575 (data not shown).

To further confirm that the TSPO PET signal originates from CNTF-activated astrocytes, we studied TSPO striatal expression by double immunostaining. We found that TSPO immunoreactivity was increased in the striatum injected with lenti-CNTF, overlapping the GFAP-positive area (Figure 6A). Cells that overexpressed TSPO in the lenti-CNTF injected striatum were strongly immunoreactive for GFAP (Figure 6A). On the contrary, there was only minimal colocalization of TSPO with CD11b-positive microglia in the same area (Figure 6B). In the contralateral side injected with lenti-LacZ, GFAP and TSPO staining were minimal (Figure 6A). This basal TSPO staining perfectly colocalized with CD11b staining, suggesting that TSPO is expressed at a low level in resting microglia (Figure 6B). A triple immunostaining against TSPO, CD11b and vimentin confirmed that TSPO was overexpressed in CNTF-activated astrocytes (Figure 6C). To evaluate whether the increase in TSPO expression in reactive astrocytes originates from an increase at the mRNA level, we performed RT-qPCR in rats injected with lenti-LacZ and lenti-CNTF in the left and right striatum respectively. CNTF induced a 4-fold increase in TSPO mRNA levels ($p < 0.05$, paired t -test, Figure 7A). Importantly TSPO mRNA levels were similar in lenti-LacZ controls and non injected controls (data not shown). We finally performed western blots on striatal protein homogenates to evaluate TSPO protein levels by densitometry. TSPO levels (normalized to actin) were significantly increased by CNTF, by a factor of 6 ($p < 0.05$, paired t -test, Figure 7A, B).

Discussion

Using a unique *in vivo* model of selective activation of astrocytes, we demonstrate that reactive astrocytes overexpress TSPO at the mRNA and protein level, which is specifically detected by PET imaging using [¹⁸F]DPA-714 and [¹¹C]SSR180575 radioligands.

The CNTF model of astrocyte activation is an original and relevant model to assess reactive astrocyte function *in vivo*. Indeed, CNTF, whose levels increase in several pathological conditions (Ip *et al.*, 1993; Haas *et al.*, 2004), binds to a tripartite receptor partially shared with many other cytokines and activates the JAK-STAT3 pathway (Escartin *et al.*, 2006). This is a central signaling pathway known to be involved in astrocyte activation (Okada *et al.*, 2006; Herrmann *et al.*, 2008). Our model is thus relevant to many pathological situations in which astrocytes become reactive upon stimulation of the JAK-STAT3 pathway. There are several additional assets to this model, especially in the context of PET studies : 1) CNTF produces a widespread activation of astrocytes throughout the striatum that is compatible with the PET spatial resolution; 2) neurons and the blood brain barrier remain unaltered and display normal anatomical and functional features (Escartin *et al.*, 2006; Beurrier *et al.*, 2010, and data not shown); 3) the contralateral hemisphere can serve as a control (being injected with lenti-LacZ), eliminating key bias for PET imaging such as variability in age, weight, peripheral metabolism of radioligands and other source of inter-individual variations, and finally; 4) activation of astrocytes is stable over time, from 15 days to at least 6 months post-injection of lenti-CNTF (Escartin *et al.*, 2006), allowing multiple imaging sessions on the same animal.

The transcriptional regulation of TSPO has rarely been evaluated in PET studies. Here, we report for the first time that CNTF induces a 4-fold increase in TSPO mRNA levels. This is consistent with other models of neuroinflammation including degeneration of the entorhinal-hippocampal perforant path (3 fold increase, Pedersen *et al.*, 2006), or focal cerebral ischemia (3 fold increase, Rojas *et al.*, 2007). CNTF overexpression in the striatum activates STAT3-dependant transcription. The TSPO promoter contains

conserved binding sequences for STAT3 in rodents and humans (Batarseh and Papadopoulos, 2010), which could mediate the transcriptional induction of TSPO by CNTF.

One of the first TSPO-selective PET radioligand to be developed and characterized for neuroinflammation imaging was [^{11}C]-(*R*)-PK11195 (Venneti *et al.*, 2006; Chauveau *et al.*, 2008). However, [^{11}C]-(*R*)-PK11195 displays some limitations *in vivo* that motivated the development of new TSPO radioligands. Multiple candidate molecules have been generated, including the indolacetamide [^{11}C]SSR180575 and the pyrazolopyrimidineacetamide [^{18}F]DPA-714 (Chauveau *et al.*, 2008; Dollé *et al.*, 2009). [^{18}F]DPA-714 has been mainly evaluated and quantified in rat models of excitotoxicity (Chauveau *et al.*, 2009) and cerebral ischemia (Martin *et al.*, 2010) while [^{11}C]SSR180575 has only been evaluated once in a rat model of excitotoxicity (Chauveau *et al.*, 2011). In addition, [^{18}F]DPA-714 was studied in the healthy primate and displayed marked uptake in TSPO-rich organs and specific binding in the brain as demonstrated using PK11195 (James *et al.*, 2008). [^{18}F]DPA-714 has been recently studied in healthy human subjects (Arlicot *et al.*, 2011) and is currently evaluated in phase I-II clinical trials in Alzheimer's disease and amyotrophic lateral sclerosis patients (clinical trials #NCT01009359 and #NCT00563537).

In our model, the two TSPO radioligands demonstrated a significantly increased and specific binding in the lenti-CNTF injected striatum. The uptake ratio between the lenti-CNTF and the lenti-LacZ-injected striata was not significantly different between [^{18}F]DPA-714 and [^{11}C]SSR180575 (respectively 2.29 and 3.35). Both radioligands were sensitive to pre-saturation and displacement with unlabeled competitive PK11195 ligand. [^{18}F]DPA-714 and [^{11}C]SSR180575 were completely displaced from the CNTF-injected striatum, reaching within minutes the uptake level measured after pre-saturation with PK11195.

Interestingly, we detected a low binding level of both TSPO radioligands in the control, lenti-LacZ injected striatum, that was also sensitive to pre-saturation and displacement with unlabeled PK11195, as already described for [^{11}C]SSR180575 (Chauveau *et al.*, 2011). This basal expression of TSPO was confirmed by RT-qPCR and was similar to the one found in non injected controls. Using double-stainings, we observed that expression of TSPO was restricted to resting microglia in the control brain. Despite this

detectable basal expression of TSPO, it was still possible to demonstrate a significant increase in radioligand binding in the lenti-CNTF striatum.

The cellular origin of the signal detected by TSPO radioligands is debated, but it is generally admitted that TSPO PET imaging reflects microglial activation in brain disease models or in patients (Cagnin *et al.*, 2002; Venneri *et al.*, 2006; 2009; Politis and Piccini, 2012). This is originally based on the observation that the temporal profiles of microglial activation and TSPO radioligand binding correlate well, as assessed by *ex vivo* autoradiography (Myers *et al.*, 1991; Pedersen *et al.*, 2006; Maeda *et al.*, 2007; Venneri *et al.*, 2007). However, using a model of hippocampal neurotoxicity, a landmark study reported that reactive astrocytes also overexpress TSPO and could contribute to TSPO radioligand binding *ex vivo* (Kuhlmann and Guilarte, 2000). This was later confirmed in other models (Chen *et al.*, 2004; Chen and Guilarte, 2006; Maeda *et al.*, 2007; Martin *et al.*, 2010), but to our knowledge, only two *in vivo* studies have reported that reactive astrocytes overexpress TSPO to levels detectable by PET imaging (Rojas *et al.*, 2007; Ji *et al.*, 2008). However, the models used (middle cerebral artery occlusion and cuprizone intoxication) induce complex pathological effects such as blood brain barrier alteration, neuronal death, demyelination and some levels of microglia activation. Such effects could impact the resultant PET signal. In our study, we aimed at isolating the contribution of reactive astrocytes to the TSPO PET signal by selectively activating astrocytes in the normal rat brain, in the absence of additional pathological processes. We were able to demonstrate that reactive astrocytes by themselves overexpress TSPO and provide a significant binding of TSPO radioligand *in vivo*.

Our findings indicate that, in complex pathological states (neurodegenerative diseases, traumatic brain injury or stroke) associated with both reactive astrocytes and microglia, the observed TSPO signal may well originate from either one or both cell types. Therefore, in absence of *postmortem* immunohistological analysis, caution must be used to conclude on the cellular origin of the TSPO PET signal and thus, on the influence of reactive glial cells on disease progression. Indeed, astrocytes and microglia play very different roles in the brain: astrocytes provide trophic support to neurons, promote

metabolic and ionic homeostasis and, regulate synaptic transmission while microglial cells are responsible for innate immune response and phagocytosis. Reactive astrocytes are known to promote neuroprotection against excitotoxic, metabolic, oxidative or even mechanical injuries (Escartin and Bonvento, 2008; Hamby and Sofroniew, 2010). In particular, CNTF-activated astrocytes protect neurons against glutamate outflow (Escartin *et al.*, 2006; Beurrier *et al.*, 2010) and metabolic deficits (Escartin *et al.*, 2007). The effect of reactive microglia on neuronal survival is more complex and controversial (Hanisch and Kettenmann, 2007). Although these cells may have beneficial effects, they typically produce high levels of pro-toxic cytokines and reactive oxygen species. It was proposed that TSPO-positive reactive astrocytes participate in a beneficial response, in contrast to TSPO-positive microglial cells that mediate more detrimental effects on neurons (Ji *et al.*, 2008).

There is now a multitude of TSPO radioligands available with different characteristics in terms of chemical classes, pharmacokinetics, peripheral metabolism and specificity towards TSPO (Chauveau *et al.*, 2008; Dollé *et al.*, 2009). It could be interesting to screen these radioligands for their capacity to discriminate between TSPO expressed by reactive astrocytes and reactive microglia, taking advantage of the CNTF model or similar models of cell-specific activation. Alternative imaging approaches may also enable discrimination of reactive astrocytes from reactive microglia, based on the preferential expression of specific proteins by either cell type. Monoamine oxidase B radioligands (Johansson *et al.*, 2007) or labeled mGluR5 agonists (Drouin-Ouellet *et al.*, 2011) are two possible candidates for PET imaging of reactive astrocytes and microglia respectively, but they need to be explored in further details.

Developing non-invasive imaging techniques to monitor neuroinflammation at the cellular level remains a crucial goal. It would contribute to the evaluation of disease models and therapeutic strategies in animals as well as the diagnosis and monitoring of various brain diseases in patients. Accurate assessment of available PET radioligands, using appropriate models of neuroinflammation like the one presented here, is a prerequisite towards this goal.

References

- Arlicot N, Vercouillie J, Ribeiro MJ, Tauber C, Venel Y, Baulieu JL, Maia S, Corcia P, Stabin MG, Reynolds A, Kassiou M, Guilloteau D (2011) Initial evaluation in healthy humans of [18F]DPA-714, a potential PET biomarker for neuroinflammation. *Nucl Med Biol.* 39:170-178.
- Batarseh A, Papadopoulos V (2010) Regulation of translocator protein 18 kDa (TSPO) expression in health and disease states. *Mol Cell Endocrinol* 327:1-12.
- Beurrier C, Faideau M, Bennouar KE, Escartin C, Kerkerian-Le Goff L, Bonvento G, Gubellini P (2010) Ciliary neurotrophic factor protects striatal neurons against excitotoxicity by enhancing glial glutamate uptake. *PLoS One* 5:e8550.
- Cagnin A, Gerhard A, Banati RB (2002) In vivo imaging of neuroinflammation. *Eur Neuropsychopharmacol* 12:581-586.
- Chauveau F, Boutin H, Van Camp N, Dolle F, Tavitian B (2008) Nuclear imaging of neuroinflammation: a comprehensive review of [11C]PK11195 challengers. *Eur J Nuc Med Mol Imag* 35:2304-2319.
- Chauveau F, Van Camp N, Dolle F, Kuhnast B, Hinnen F, Damont A, Boutin H, James M, Kassiou M, Tavitian B (2009) Comparative evaluation of the translocator protein radioligands 11C-DPA-713, 18F-DPA-714, and 11C-PK11195 in a rat model of acute neuroinflammation. *J Nucl Med* 50:468-476.
- Chauveau F, Boutin H, Van Camp N, Thominiaux C, Hantraye P, Rivron L, Marguet F, Castel MN, Rooney T, Benavides J, Dolle F, Tavitian B (2011) In vivo imaging of neuroinflammation in the rodent brain with [11C]SSR180575, a novel indoleacetamide radioligand of the translocator protein (18 kDa). *European Journal of Nuclear Medicine and Molecular Imaging* 38:509-514.
- Chen MK, Guilarte TR (2006) Imaging the peripheral benzodiazepine receptor response in central nervous system demyelination and remyelination. *Toxicol Sci* 91:532-539.
- Chen MK, Guilarte TR (2008) Translocator protein 18 kDa (TSPO): molecular sensor of brain injury and repair. *Pharmacol Ther* 118:1-17.

- Chen MK, Baidoo K, Verina T, Guilarte TR (2004) Peripheral benzodiazepine receptor imaging in CNS demyelination: functional implications of anatomical and cellular localization. *Brain* 127:1379-1392.
- Damont A, Hinnen F, Kuhnast B, Schollhorn-Peyronneau MA, James M, Luus C, Tavitian B, Kassiou M, Dolle F (2008) Radiosynthesis of [18F]DPA-714, a selective radioligand for imaging the translocator protein (18 kDa) with PET. *J Label Compds Radiopharm* 51:286-292.
- Dollé F, Luus C, Reynolds A, Kassiou M (2009) Radiolabelled molecules for imaging the translocator protein (18 kDa) using positron emission tomography. *Curr Med Chem* 16:2899-2923.
- Drouin-Ouellet J, Brownell AL, Saint-Pierre M, Fasano C, Emond V, Trudeau LE, Levesque D, Cicchetti F (2011) Neuroinflammation is associated with changes in glial mGluR5 expression and the development of neonatal excitotoxic lesions. *Glia* 59:188-199.
- Dubois A, Dauguet J, Herard AS, Besret L, Duchesnay E, Frouin V, Hantraye P, Bonvento G, Delzescaux T (2007) Automated three-dimensional analysis of histological and autoradiographic rat brain sections: application to an activation study. *J Cereb Blood Flow Metab* 27:1742-1755.
- Escartin C, Bonvento G (2008) Targeted activation of astrocytes: a potential neuroprotective strategy. *Mol Neurobiol* 38:231-241.
- Escartin C, Won SJ, Malgorn C, Auregan G, Berman AE, Chen PC, Deglon N, Johnson JA, Suh SW, Swanson RA (2011) Nuclear factor erythroid 2-related factor 2 facilitates neuronal glutathione synthesis by upregulating neuronal excitatory amino acid transporter 3 expression. *J Neurosci* 31:7392-7401.
- Escartin C, Brouillet E, Gubellini P, Trioulier Y, Jacquard C, Smadja C, Knott GW, Kerkerian-Le Goff L, Deglon N, Hantraye P, Bonvento G (2006) Ciliary neurotrophic factor activates astrocytes, redistributes their glutamate transporters GLAST and GLT-1 to raft microdomains, and improves glutamate handling in vivo. *J Neurosci* 26:5978-5989.

Escartin C, Pierre K, Colin A, Brouillet E, Delzescaux T, Guillermier M, Dhenain M, Deglon N, Hantraye P, Pellerin L, Bonvento G (2007) Activation of astrocytes by CNTF induces metabolic plasticity and increases resistance to metabolic insults. *J Neurosci* 27:7094-7104.

Haas SJ, Ahrens A, Petrov S, Schmitt O, Wree A (2004) Quinolinic acid lesions of the caudate putamen in the rat lead to a local increase of ciliary neurotrophic factor. *J Anat* 204:271-281.

Hamby ME, Sofroniew MV (2010) Reactive astrocytes as therapeutic targets for CNS disorders. *Neurotherapeutics* 7:494-506.

Hanisch UK, Kettenmann H (2007) Microglia: active sensor and versatile effector cells in the normal and pathologic brain. *Nat Neurosci* 10:1387-1394.

Herrmann JE, Imura T, Song B, Qi J, Ao Y, Nguyen TK, Korsak RA, Takeda K, Akira S, Sofroniew MV (2008) STAT3 is a critical regulator of astrogliosis and scar formation after spinal cord injury. *J Neurosci* 28:7231-7243.

Ip NY, Wiegand SJ, Morse J, Rudge JS (1993) Injury-induced regulation of ciliary neurotrophic factor mRNA in the adult rat brain. *Eur J Neurosci* 5:25-33.

James ML, Fulton RR, Vercoullie J, Henderson DJ, Garreau L, Chalon S, Dolle F, Costa B, Guilloteau D, Kassiou M (2008) DPA-714, a new translocator protein-specific ligand: synthesis, radiofluorination, and pharmacologic characterization. *J Nucl Med* 49:814-822.

Ji B, Maeda J, Sawada M, Ono M, Okauchi T, Inaji M, Zhang MR, Suzuki K, Ando K, Staufienbiel M, Trojanowski JQ, Lee VM, Higuchi M, Suhara T (2008) Imaging of peripheral benzodiazepine receptor expression as biomarkers of detrimental versus beneficial glial responses in mouse models of Alzheimer's and other CNS pathologies. *J Neurosci* 28:12255-12267.

Johansson A, Engler H, Blomquist G, Scott B, Wall A, Aquilonius SM, Langstrom B, Askmark H (2007) Evidence for astrocytosis in ALS demonstrated by [11C](L)-deprenyl-D2 PET. *J Neurol Sci* 255:17-22.

- Kuhlmann AC, Guilarte TR (2000) Cellular and subcellular localization of peripheral benzodiazepine receptors after trimethyltin neurotoxicity. *J Neurochem* 74:1694-1704.
- Maeda J, Higuchi M, Inaji M, Ji B, Haneda E, Okauchi T, Zhang MR, Suzuki K, Suhara T (2007) Phase-dependent roles of reactive microglia and astrocytes in nervous system injury as delineated by imaging of peripheral benzodiazepine receptor. *Brain Res* 1157:100-111.
- Martin A, Boisgard R, Theze B, Van Camp N, Kuhnast B, Damont A, Kassiou M, Dolle F, Tavitian B (2010) Evaluation of the PBR/TSPO radioligand [18F]DPA-714 in a rat model of focal cerebral ischemia. *J Cereb Blood Flow Metab* 30:230-241.
- Myers R, Manjil LG, Cullen BM, Price GW, Frackowiak RS, Cremer JE (1991) Macrophage and astrocyte populations in relation to [3H]PK 11195 binding in rat cerebral cortex following a local ischaemic lesion. *J Cereb Blood Flow Metab* 11:314-322.
- Okada S, Nakamura M, Katoh H, Miyao T, Shimazaki T, Ishii K, Yamane J, Yoshimura A, Iwamoto Y, Toyama Y, Okano H (2006) Conditional ablation of Stat3 or Socs3 discloses a dual role for reactive astrocytes after spinal cord injury. *Nat Med* 12:829-834.
- Ourselin S, Roche A, Subsol G, Pennec X, Ayache N (2001) Reconstructing a 3D structure from serial histological sections. *Image and Vision Computing* 19:25-31.
- Pedersen MD, Minuzzi L, Wirenfeldt M, Meldgaard M, Slidsborg C, Cumming P, Finsen B (2006) Up-regulation of PK11195 binding in areas of axonal degeneration coincides with early microglial activation in mouse brain. *Eur J Neurosci* 24:991-1000.
- Politis M, Piccini P (2012) Positron emission tomography imaging in neurological disorders. *J Neurol*. In press
- Rojas S, Martin A, Arranz MJ, Pareto D, Purroy J, Verdaguer E, Llop J, Gomez V, Gispert JD, Millan O, Chamorro A, Planas AM (2007) Imaging brain inflammation with [11C]PK11195 by PET and induction of the peripheral-type benzodiazepine receptor after transient focal ischemia in rats. *J Cereb Blood Flow Metab* 27:1975-1986.

- Rupprecht R, Papadopoulos V, Rammes G, Baghai TC, Fan J, Akula N, Groyer G, Adams D, Schumacher M (2010) Translocator protein (18 kDa) (TSPO) as a therapeutic target for neurological and psychiatric disorders. *Nat Rev Drug Discov* 9:971-988.
- Ryu JK, Choi HB, McLarnon JG (2005) Peripheral benzodiazepine receptor ligand PK11195 reduces microglial activation and neuronal death in quinolinic acid-injected rat striatum. *Neurobiol Dis* 20:550-561.
- Thominiaux C, Damont A, Kuhnast B, Demphel S, Le Helleix S, Boisnard S, Rivron L, Chauveau F, Boutin H, Van Camp N, Boisgard R, Roy S, Allen J, Rooney T, Benavides J, Hantraye P, Tavitian B, Dolle F (2010) Radiosynthesis of 7-chloro-N,N-dimethyl-5-[¹¹C]methyl-4-oxo-3-phenyl-3,5-dihydro-4H-pyridazino[4,5-b]indole-1-acetamide, [¹¹C]SSR180575, a novel radioligand for imaging the TSPO (peripheral benzodiazepine receptor) with PET. *J Label Compds Radiopharm* 53:767-773.
- Venneti S, Lopresti BJ, Wiley CA (2006) The peripheral benzodiazepine receptor (Translocator protein 18kDa) in microglia: from pathology to imaging. *Prog Neurobiol* 80:308-322.
- Venneti S, Wiley CA, Kofler J (2009) Imaging microglial activation during neuroinflammation and Alzheimer's disease. *J Neuroimmune Pharmacol* 4:227-243.
- Venneti S, Lopresti BJ, Wang G, Slagel SL, Mason NS, Mathis CA, Fischer ML, Larsen NJ, Mortimer AD, Hastings TG, Smith AD, Zigmond MJ, Suhara T, Higuchi M, Wiley CA (2007) A comparison of the high-affinity peripheral benzodiazepine receptor ligands DAA1106 and (R)-PK11195 in rat models of neuroinflammation: implications for PET imaging of microglial activation. *J Neurochem* 102:2118-2131.

Legends to Figures and Tables

Figure 1. CNTF selectively activates astrocytes

A. CNTF increases mRNA levels of GFAP and vimentin but has no significant effects on microglia markers IBA1 and CD11b. mRNA levels were normalized to cyclophilin and expressed relatively to levels in the LacZ group (set at 100%). $N = 5$, $** p < 0.005$ paired t -test. **B - E.** Immunostainings of rat brains injected with lenti-LacZ and lenti-CNTF in the left and right striatum, respectively. CNTF increases the expression of the astrocyte intermediate filaments GFAP (**B**) and vimentin (**C**). At higher magnification, astrocytes display the characteristic reactive hypertrophic morphology (**D**). In comparison to astrocytes, CNTF has limited effects on microglial cells detected by their expression of IBA1. (**E**) ED1/CD68, a selective marker of reactive microglia, is expressed at background level in both striata. Scale bars = 2.5 mm and 50 μm . Sections are counterstained with Hematoxylin/Blueing. **F.** Staining intensity measured in the striatum injected with lenti-LacZ or lenti-CNTF after background subtraction. $N = 6$ rats with 6-8 sections for each rat. $* p < 0.05$, $** p < 0.005$, $*** p < 0.001$, paired t -test. **G.** Immunofluorescent stainings for GFAP and IBA1 confirm that CNTF induces strong morphological changes in astrocytes but not in microglia, as compared to the positive control brain injected with quinolinate (QA). Scale bar = 10 μm .

Figure 2. [^{18}F]DPA-714 and [^{11}C]SSR180575 bind to the lenti-CNTF injected striatum

Coronal rat brain view of %SUV summed PET images (over 90 min) for [^{18}F]DPA-714 (**A**) and [^{11}C]SSR180575 (**B**), after co-registration with the individual MRI. A large area of radioligand binding is observed in the striatum injected with lenti-CNTF for both radioligands. TACs for [^{18}F]DPA-714 (**C**, $n = 6$) and [^{11}C]SSR180575 (**D**, $n = 4$) in the lenti-CNTF and the contralateral lenti-LacZ-injected striata. TACs are expressed as mean %SUV. Both radioligands displayed a strong significant difference between the lenti-CNTF and lenti-LacZ striata ($p < 10^{-4}$ for both radioligands, two-way repeated-measures ANOVA). Color-coded scale is in Bq/cm^3 .

Figure 3. [¹⁸F]DPA-714 and [¹¹C]SSR180575 binding is pre-saturated and displaced by an excess of PK11195

A-B. Pre-saturation of [¹⁸F]DPA-714 and [¹¹C]SSR180575 was tested with an injection of respectively 2 and 5 mg/kg of PK11195, 5 min before radioligand administration. Displacement of [¹⁸F]DPA-714 and [¹¹C]SSR180575 was induced by 1 mg/kg of PK11195, respectively 15 and 20 min following radioligand administration (arrow). TACs are shown for [¹⁸F]DPA-714 (**A**) and [¹¹C]SSR180575 (**B**) on both lenti-CNTF and lenti-LacZ striata. An additional baseline experiment is shown; all three exams were performed on the same rat for each radioligand.

Figure 4. Representative PET images of [¹⁸F]DPA-714 pre-saturation and displacement

Coronal rat brain views of [¹⁸F]DPA-714 %SUV summed PET images (over 90 min), co-registered with the individual MRI under baseline (**A**), pre-saturation (**B**) and displacement conditions (**C**: %SUV summed image over first 15 min, **D** : %SUV summed image over last 75 min). Color-coded scale is in Bq/cm³.

Figure 5. GFAP-positive histological volume matches the radioligand binding volume

Rats were subjected to [¹⁸F]DPA-714 PET and MRI scans (**B**, **D**, **F1**, **F2**), and had their brains cut and processed for GFAP-immunohistochemistry (**A**, **C**, **E1**, **E2**). PET and MRI 3D images were co-registered to provide fusion images as shown in **B** (coronal view), **D** (axial view), **F1** (left sagittal view) and **F2** (right sagittal view). During brain cutting, block face photographs were taken in order to reconstruct the *postmortem* brain in 3D and to allow superimposition of digitised and 3D-reconstructed GFAP-stained sections (lighter band in **C**, **E1**, **E2**). A strong correspondence between GFAP-positive histological volume and [¹⁸F]DPA-714 PET signal is observed in the right striatum injected with lenti-CNTF. Color-coded scale is in Bq/cm³.

Figure 6. TSPO is overexpressed by CNTF-activated astrocytes

A. In the striatum injected with lenti-LacZ, there is a low level of staining for GFAP (red) and TSPO (green). The needle track is indicated by a star. In the striatum injected with lenti-CNTF, TSPO staining is very intense and matches the area displaying GFAP-positive reactive astrocytes (area left to dashes). TSPO is expressed at the highest level in GFAP-positive astrocytes (white arrowhead). Scale bars = 20 μm . **B.** On the contrary, in the lenti-CNTF injected striatum, there is only a limited colocalization of TSPO (green) with CD11b-labeled microglia (red, open arrowheads). Such colocalization is also observed in the control striatum injected with lenti-LacZ and gives rise to minimal PET signal. CD11b staining is not visibly enhanced in the area with reactive astrocytes (area above dashes). Scale bars = 20 μm . **C.** At higher magnification in the lenti-CNTF injected striatum, vimentin-positive reactive astrocytes (blue, white arrowhead) express high level of TSPO (green), contrary to CD11b-labeled microglia (red, open arrowhead) that express undetectable levels of TSPO. Scale bars = 10 μm .

Figure 7. TSPO expression is increased by CNTF

Striatal samples from rats injected with lenti-LacZ (LacZ, L) and lenti-CNTF (CNTF, C) in the left and right striatum respectively were analyzed by RT-qPCR and western blot. **A.** CNTF significantly increases TSPO expression. TSPO mRNA and protein levels were normalized to cyclophilin and actin respectively and expressed relatively to levels in the LacZ group (set at 1). N = 5 and N = 3 respectively, * $p < 0.05$, paired t -test. **B.** Representative western blot for TSPO.

Table 1. CNTF activates astrocytes and has limited effects on other neuroinflammation markers

Analysis by RT-qPCR array of the expression of 22 genes related to neuroinflammation in rats injected with lenti-LacZ or lenti-CNTF. mRNA levels of all genes were normalized to actin mRNA levels and expressed relatively to the LacZ group (set at 100%). N = 5, * $p < 0.05$, ** $p < 0.005$, paired *t*-test.

Table 1

Gene Symbol (common name)	Seq #	mRNA level	
		Lenti-LacZ	Lenti-CNTF
Astrocytes			
Gfap	NM_017009	100 ± 20.95	1 272.89 ± 144.83 **
Vim (Vimentin)	NM_031140	100 ± 23.15	830.81 ± 121.58 **
Microglia			
Itgam (CD11b)	NM_012711	100 ± 12.67	165.78 ± 34.27
Aif1 (IBA1)	NM_017196	100 ± 13.65	138.95 ± 12.83
Cytokines & chemokines			
IL-1a	NM_017019	100 ± 7.71	125.22 ± 26.98
IL-6	NM_012589	100 ± 10.68	97.39 ± 14.57
IL-10	NM_012854	100 ± 19.31	96.26 ± 21.57
LIF	NM_022196	100 ± 15.70	82.28 ± 17.17
OSM (Oncostatin M)	NM_001006961	100 ± 23.39	128.47 ± 23.40
Tnfa (TNFalpha)	NM_012675	100 ± 13.04	200.56 ± 34.05 *
Ccl3 (MIP1-alpha)	NM_013025	100 ± 9.53	57.53 ± 19.34
Ccl5 (RANTES)	NM_031116	100 ± 29.48	82.54 ± 34.32
Cxcl1 (GRO/KC)	NM_030845	100 ± 17.57	61.72 ± 5.24
C3	NM_016994	100 ± 19.54	127.33 ± 32.83
Oxidative stress			
Ncf1 (p47phox)	NM_053734	100 ± 13.95	109.77 ± 17.44
Ncf2 (p67phox)	XM_344156	100 ± 22.58	95.16 ± 4.84 *
Nox4	NM_053524	100 ± 23.74	95.65 ± 30.43
Noxa1	XM_231042	100 ± 29.41	117.65 ± 11.76 **
Noxo1	XM_220221	100 ± 21.74	65.22 ± 21.76
Nos2 (iNOS)	NM_012611	100 ± 52.05	76.64 ± 36.82
Ptgs1 (Cyclooxygenase 1)	NM_017043	100 ± 8.62	115.52 ± 8.62
Ptgs2 (Cyclooxygenase 2)	NM_017232	100 ± 15.46	76.81 ± 6.76 **

Figure 1

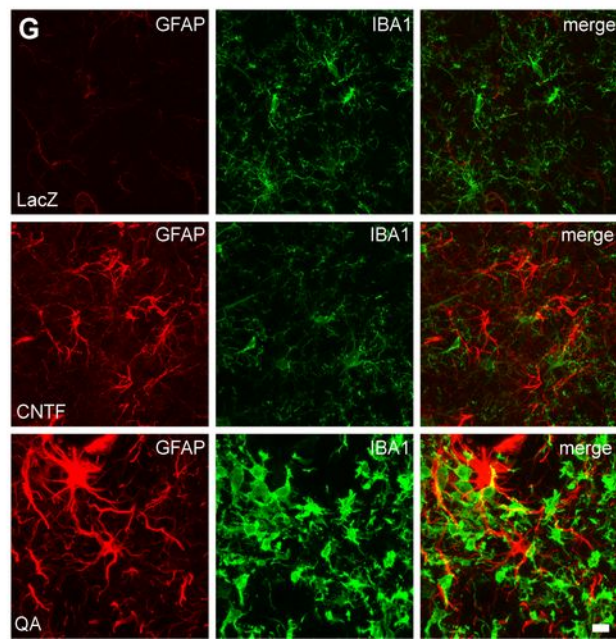
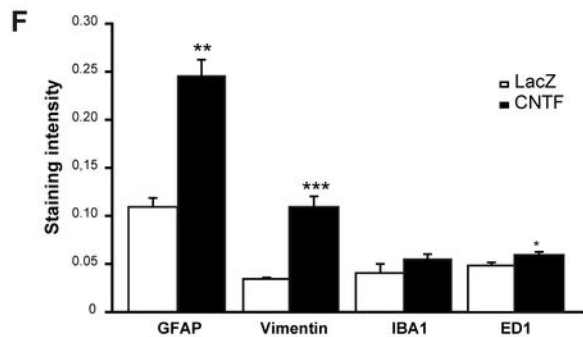
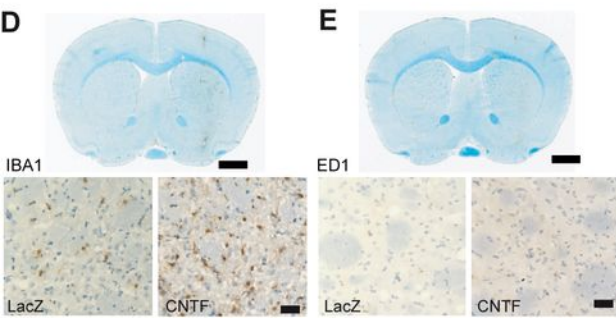
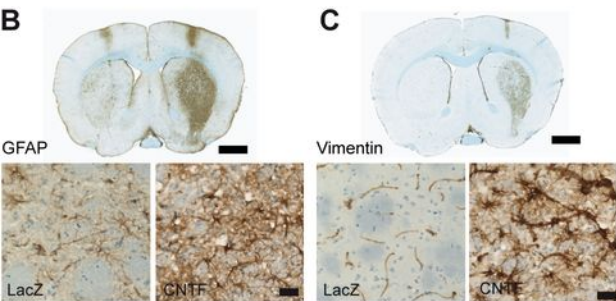
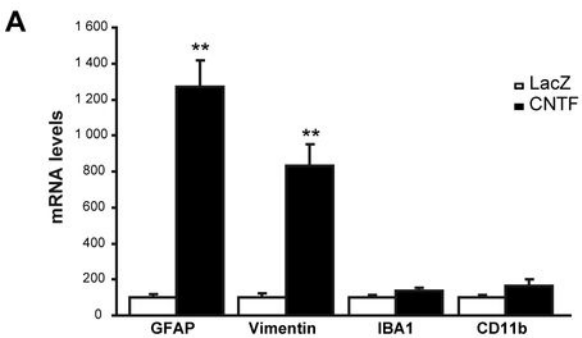
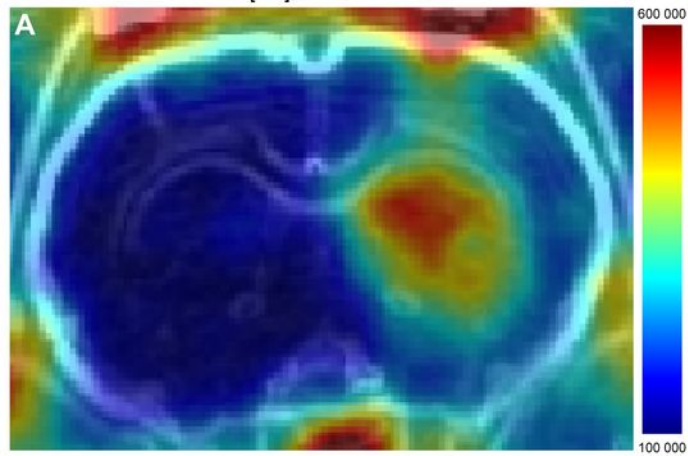


Figure 2

[¹⁸F]DPA-714



[¹¹C]SSR180575

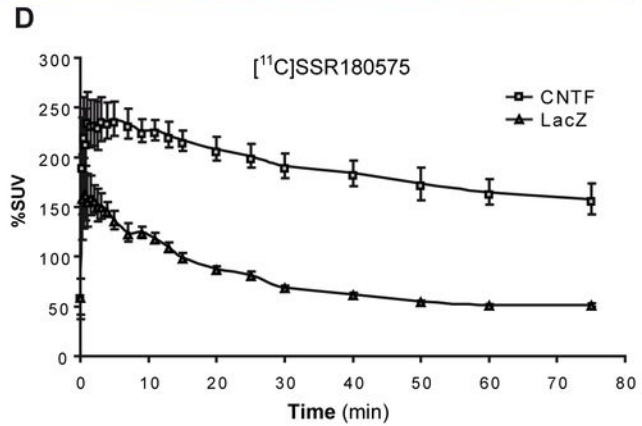
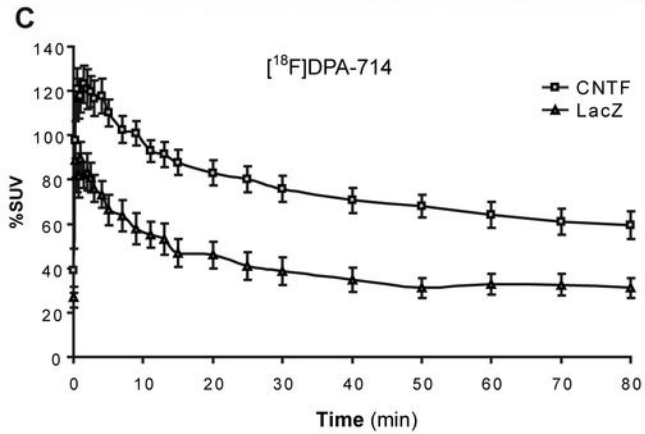
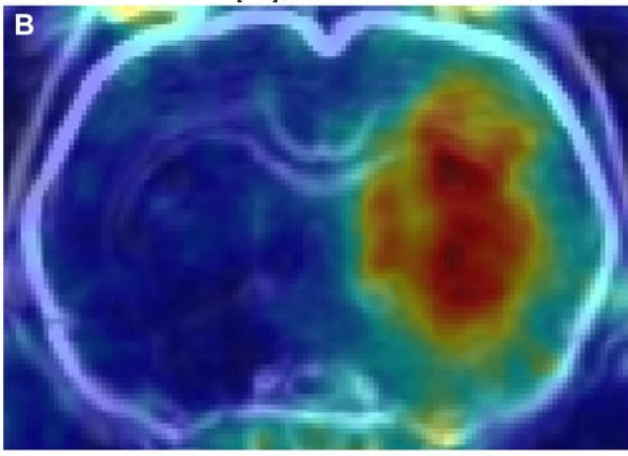


Figure 3

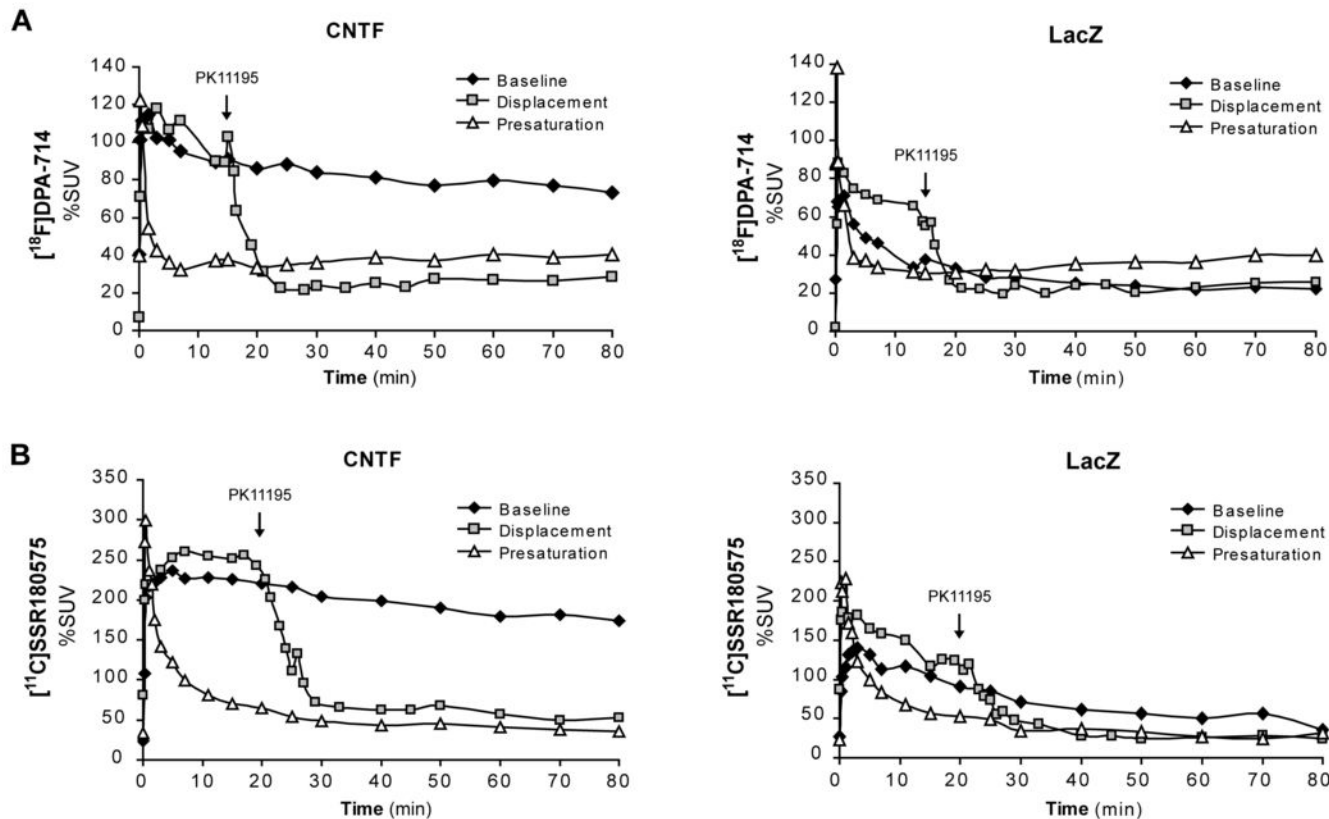


Figure 4

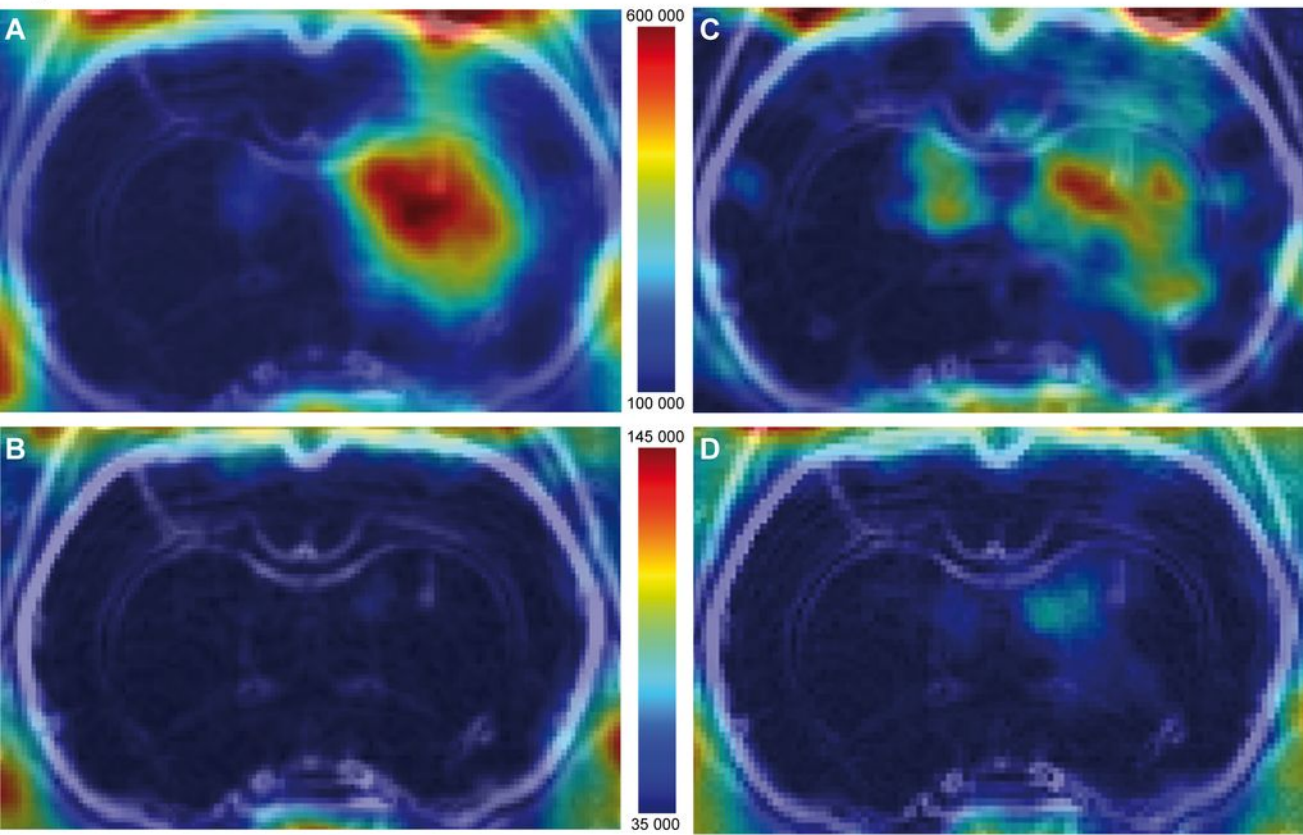


Figure 5

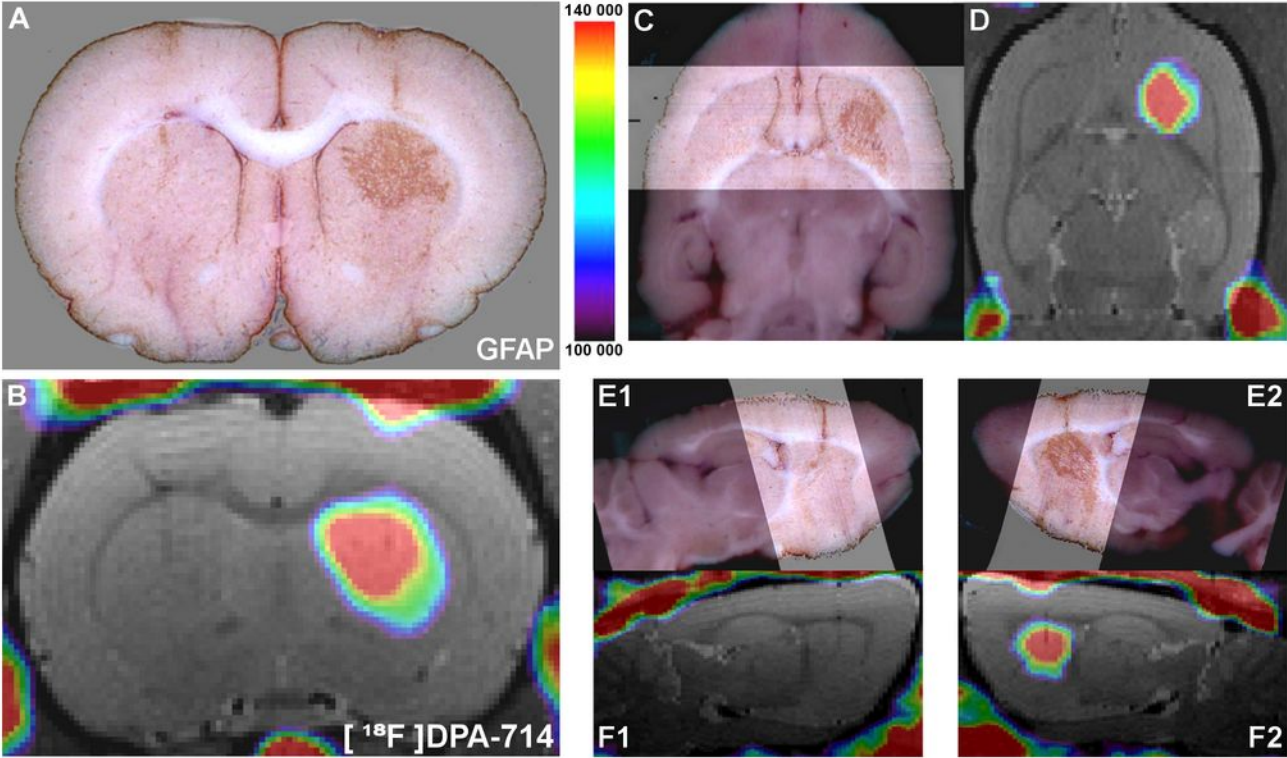


Figure 6

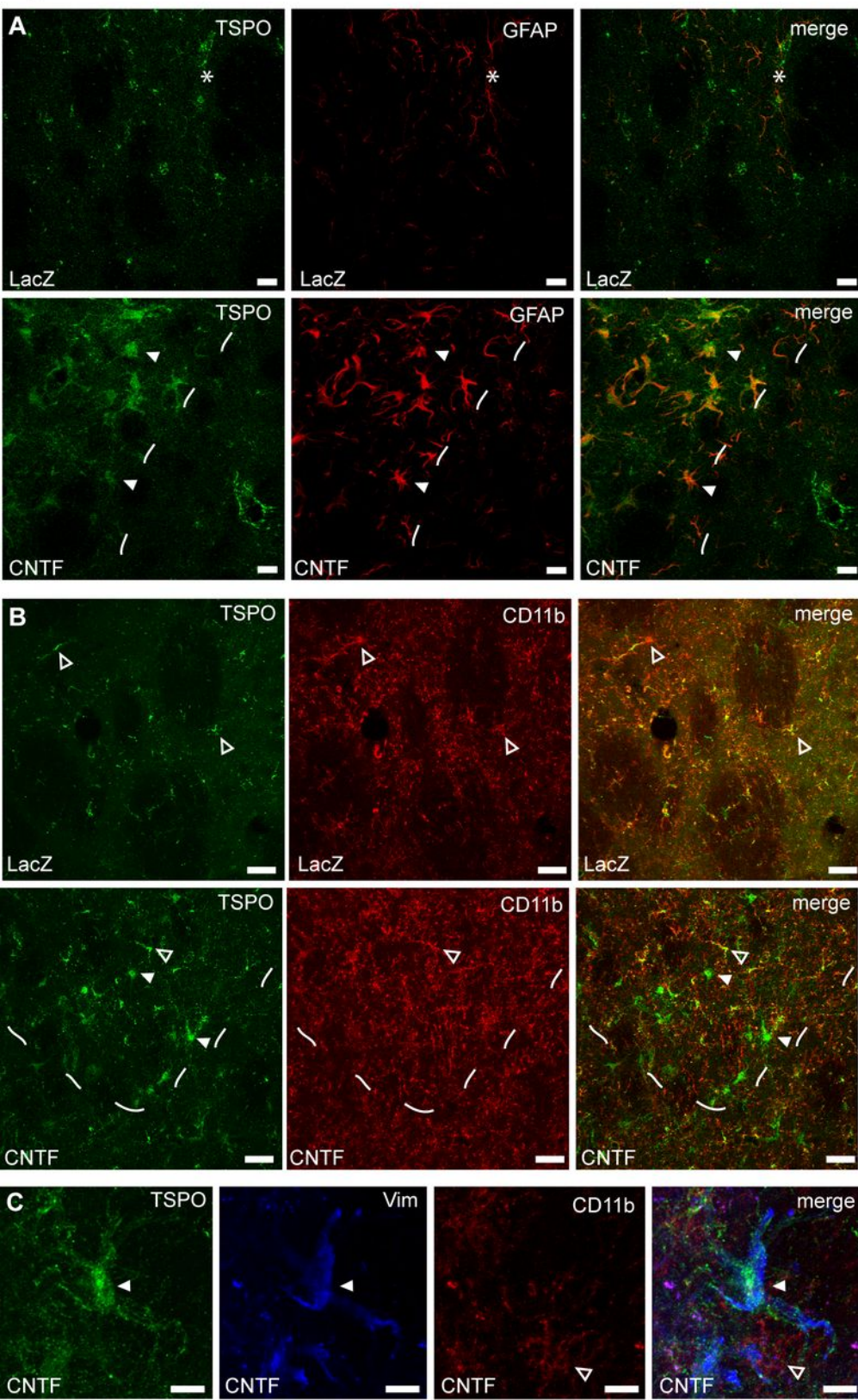
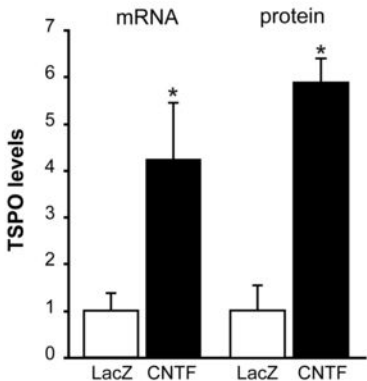


Figure 7

A



B

